Dear Olivier,
in the following we comment on each remark. In normal font you find the original comments, in bold our response. 'Done.' denotes that this point has been solved. This could be that it has been either done directly, or that due to other changes the point does not arise any more, or that the point has been answered at another place in this text already.

Again, many thanks for all the very helpful suggestions!

Best regards,

Nina and co-authors

Editor comments

- page 3, line 17: 'we believe' doesn't sound very scientific? Especially when in the next sentence you use 'therefore'. I would suggest to rewrite these two sentences.
We agree and have removed: "We believe the basal sliding behaviour is a similarly important process as is the lateral buttressing.", as we already stated the importance of basal sliding in the text above.

- I have some issue with the BC at the base. Can you confirm that the Dirichlet BC (8; u.n=0) is only applied where the ice is grounded (not under the ice shelf)?
It is applied to the whole base. See the sentence
"This Dirichlet condition is applied to the entire ice base, including grounded and floating parts, and also implies that no basal melting is considered." after the boundary condition. We have rewritten the BC part (see your comment to Equation 14).

Then, my experience is that applying in the normal direction the hydrostatic pressure below the ice shelf is not stable. This is not stable as a very small shift from the hydrostatic equilibrium will induce very large normal velocity (if the bottom surface is too low, the whole ice-shelf is pushed up, and the reverse if it is to high). In our case, we have to had a 'viscous spring' which account for the fact that the sea water pressure is a function of the altitude (see for example Durand et al., 2009).
Yes, we figured out the same problem in prognostic simulations.

I am therefore wondering if you are not applying u/n=0 below the ice shelf since you are solving a diagnostic problem?
See above.

- Equation 12: for a Stokes problem, the normal stress is not equal to the cryospheric pressure. To evaluate the overburden pressure you should use the normal stress from your Stokes solution.
We agree, in a full Stokes system the pressure contains a cryostatic and a dynamic part. In general, the dynamic part is small compared the cryostatic part, even if the bed is rough or sliding is changing over short distances as shown by all models in the ISMIP-HOM experiments (see Dp figures in the supplement: http://www.the-cryosphere. net/2/95/2008/tc-2-95-2008-supplement.zip). We have implemented the parameterization according to Huybrechts (1992). We added "Eq 13 further implies, that the overburden pressure is cryostatic and neglects the dynamic contribution from the Stokes solution to the pressure. In general, the dynamic part is small compared the cryostatic part, even if the bed is rough or sliding is changing over short distances \citep[][supplementary material]{Pattyn_et_al_2008}." in the updated

manuscript.

- Equation 14: you should specify at which base is applied this equation. Grounded or floating. In any case this seems false for me. For the floating part, only the normal pressure should be applied (+ the viscous spring to make it stable) and for the grounded part, the BC are u.n=0 and the friction law... (so that the normal stress is not acting in the FE formulation, i.e. you can not have a Dirichlet and a Neumann BC applied at the same time in the same direction, the Dirichlet only will apply in that case).

Yes, you are right. The description of the boundary conditions is a bit confusing. As we have prescribed u.n=0 at the whole base, Eq. 9 will be overwritten (Dirichlet takes precedence). The description of the boundary condition is rewritten in the updated manuscript.

- Equation 20: I am a bit annoyed here since you claim in the introduction that with your physical method you will avoid using inverse method, but at the end you need observed surface velocity to calibrate C_b, in the same way you have used them to 'inverse' \beta...

We apologize that you are annoyed. However, we do not claim, that we avoid any kind of inversion in our study. We use a very simple inversion method to calibrate C_b and C_L in the single-parameter and two-parameter roughness approach, respectively. Compared to an inversion only approach, our approach enables us to study the effect of roughness on the flow in a subsequent experiment. We slightly rewritten one sentence to "In subsequent experiments we introduce two methods of connecting basal roughness measures to the parametrisation of basal sliding and therefore constrain basal sliding with MORE physically justified assumptions."

- page 18, line 25: should be C_b(\xi) as C_\xi has not yet been defined (next sentence).
Done.

- page 24, line 5: might also be due to the fact that you are solving for a diagnostic with no relaxation... and that the geometry (surf, bed, GL) is not consistent with the flow?
Yes, we agree and add this to the updated manuscript.

- Figure 7: how do you explain these features (patch of high T going up to the surface)? I suspect the diagnostic velocity field with a non relaxed observed surface topography to cause strange vertical velocity patterns. Did you check the vertical velocity field?
Yes, we agree, that solving for a diagnostic velocity field with no relaxation of surface topography may cause strange patterns in vertical velocity (Calov, 1994). However, we have checked the vertical velocity field, it does not show any strange pattern and the amplitudes are lower (in most of the areas several orders of magnitude) than the horizontal surface velocity. Indeed, warmer ice can be found that reachs relatively high up. The chosen colormap for temperature may suggests a very high contrast in temperatures as colour changes from light blue to dark blue (high visual contrast) within a only few degrees (e.g. -13 to -15°C "patch" temperature while the surface is around -18°C). Further, it is hard to judge where the high temperatures come from, especially, if a 2d vertical slice is not orientated along the flow direction.

- Figures 8 and 10 are too small.

Done. We have tightened the vertical axis of each subfigure. If that is not enough we will split/rearrange the figures.

Dear Olivier,
in the following we comment on each remark. In normal font you find the original comments, in bold our response. 'Done.' denotes that this point has been solved. This could be that it has been either done directly, or that due to other changes the point does not arise any more, or that the point has been answered at another place in this text already.

Again, many thanks for all the very helpful suggestions!

Best regards,

Nina and co-authors

Editor comments

- page 3, line 17: 'we believe' doesn't sound very scientific? Especially when in the next sentence you use 'therefore'. I would suggest to rewrite these two sentences.
We agree and have removed: "We believe the basal sliding behaviour is a similarly important process as is the lateral buttressing.", as we already stated the importance of basal sliding in the text above.

- I have some issue with the BC at the base. Can you confirm that the Dirichlet BC (8; u.n=0) is only applied where the ice is grounded (not under the ice shelf)?
It is applied to the whole base. See the sentence
"This Dirichlet condition is applied to the entire ice base, including grounded and floating parts, and also implies that no basal melting is considered." after the boundary condition. We have rewritten the BC part (see your comment to Equation 14).

Then, my experience is that applying in the normal direction the hydrostatic pressure below the ice shelf is not stable. This is not stable as a very small shift from the hydrostatic equilibrium will induce very large normal velocity (if the bottom surface is too low, the whole ice-shelf is pushed up, and the reverse if it is to high). In our case, we have to had a 'viscous spring' which account for the fact that the sea water pressure is a function of the altitude (see for example Durand et al., 2009).
Yes, we figured out the same problem in prognostic simulations.

I am therefore wondering if you are not applying u/n=0 below the ice shelf since you are solving a diagnostic problem?
See above.

- Equation 12: for a Stokes problem, the normal stress is not equal to the cryospheric pressure. To evaluate the overburden pressure you should use the normal stress from your Stokes solution.
We agree, in a full Stokes system the pressure contains a cryostatic and a dynamic part. In general, the dynamic part is small compared the cryostatic part, even if the bed is rough or sliding is changing over short distances as shown by all models in the ISMIP-HOM experiments (see Dp figures in the supplement: http://www.the-cryosphere. net/2/95/2008/tc-2-95-2008-supplement.zip). We have implemented the parameterization according to Huybrechts (1992). We added "Eq 13 further implies, that the overburden pressure is cryostatic and neglects the dynamic contribution from the Stokes solution to the pressure. In general, the dynamic part is small compared the cryostatic part, even if the bed is rough or sliding is changing over short distances \citep[][supplementary material]{Pattyn_et_al_2008}." in the updated

manuscript.

- Equation 14: you should specify at which base is applied this equation. Grounded or floating. In any case this seems false for me. For the floating part, only the normal pressure should be applied (+ the viscous spring to make it stable) and for the grounded part, the BC are u.n=0 and the friction law... (so that the normal stress is not acting in the FE formulation, i.e. you can not have a Dirichlet and a Neumann BC applied at the same time in the same direction, the Dirichlet only will apply in that case).
Yes, you are right. The description of the boundary conditions is a bit confusing. As we have prescribed u.n=0 at the whole base, Eq. 9 will be overwritten (Dirichlet takes precedence). The description of the boundary condition is rewritten in the updated manuscript.

- Equation 20: I am a bit annoyed here since you claim in the introduction that with your physical method you will avoid using inverse method, but at the end you need observed surface velocity to calibrate C_b, in the same way you have used them to 'inverse' \beta...
We apologize that you are annoyed. However, we do not claim, that we avoid any kind of inversion in our study. We use a very simple inversion method to calibrate C_b and C_L in the single-parameter and two-parameter roughness approach, respectively. Compared to an inversion only approach, our approach enables us to study the effect of roughness on the flow in a subsequent experiment. We slightly rewritten one sentence to "In subsequent experiments we introduce two methods of connecting basal roughness measures to the parametrisation of basal sliding and therefore constrain basal sliding with MORE physically justified assumptions."

- page 18, line 25: should be C_b(\xi) as C_\xi has not yet been defined (next sentence).
Done.

- page 24, line 5: might also be due to the fact that you are solving for a diagnostic with no relaxation... and that the geometry (surf, bed, GL) is not consistent with the flow?
Yes, we agree and add this to the updated manuscript.

- Figure 7: how do you explain these features (patch of high T going up to the surface)? I suspect the diagnostic velocity field with a non relaxed observed surface topography to cause strange vertical velocity patterns. Did you check the vertical velocity field?
Yes, we agree, that solving for a diagnostic velocity field with no relaxation of surface topography may cause strange patterns in vertical velocity (Calov, 1994). However, we have checked the vertical velocity field, it does not show any strange pattern and the amplitudes are lower (in most of the areas several orders of magnitude) than the horizontal surface velocity. Indeed, warmer ice can be found that reachs relatively high up. The chosen colormap for temperature may suggests a very high contrast in temperatures as colour changes from light blue to dark blue (high visual contrast) within a only few degrees (e.g. -13 to -15°C "patch" temperature while the surface is around -18°C). Further, it is hard to judge where the high temperatures come from, especially, if a 2d vertical slice is not orientated along the flow direction.

- Figures 8 and 10 are too small.

Done. We have tightened the vertical axis of each subfigure. If that is not enough we will split/rearrange the figures.

Thermal structure and basal sliding parametrisation at Pine Island Glacier - a 3D full-Stokes model study

N. Wilkens[1,2]**, J. Behrens**[3]**, T. Kleiner**[2]**, D. Rippin**[4]**, M. Rückamp**[2]**, and A. Humbert**[2,5]

[1]Institute for Geophysics, University of Hamburg, Germany
[2]Alfred Wegener Institute, Helmholtz Centre for Polar and Marine Research, Bremerhaven, Germany
[3]Numerical Methods in Geosciences, University of Hamburg, Germany
[4]Environment Department, University of York, Heslington, UK
[5]Department of Geosciences, University of Bremen, Germany

Correspondence to: Nina Wilkens (nina.wilkens@zmaw.de)

Abstract

Pine Island Glacier is one of the fastest changing glaciers in the Antarctic Ice Sheet and therefore in scientific focus. The glacier holds enough ice to raise global sea level significantly (~ 0.5 m), when fully melted. The question addressed by numerous modelling studies of the glacier focusses on whether the observed changes are a start for an uncontrolled and accelerating retreat. The movement of the glacier is, in the fast flowing areas, dominated by basal motion. In modelling studies the parametrisation of the basal motion is therefore crucial. Inversion methods are commonly applied to reproduce the complex surface flow structure at Pine Island Glacier, which use information of the observed surface velocity field, to constrain, among other things, basal sliding. We introduce two different approaches of combining a physical parameter, the basal roughness, with basal sliding parametrisations. This way basal sliding is connected again closer to its original formulation. We show that the basal roughness is an important and helpful parameter to consider and that many features of the flow structure can be reproduced with these approaches.

1 Introduction

In the past decades the fastest changes in ice flow velocity, ice thickness and grounding line retreat in the Antarctic Ice Sheet have been observed in the region of Pine Island Glacier (PIG), Amundsen Sea Embayment, West Antarctica (Rignot, 2008; Wingham et al., 2009; Rignot, 1998; Joughin et al., 2010; Park et al., 2013; Helm et al., 2014). Additionally, the currently observed mass loss from the Antarctic Ice Sheet is also concentrated in the area around PIG (Horwath and Dietrich, 2009; Shepherd et al., 2012). Thus PIG shows an increased contribution to global sea level rise (Mouginot et al., 2014).

The bed lies below sea level in large areas, making it part of a so called marine ice sheet. In combination with a retrograde bed, which slopes down from the ocean towards the center of the glacier, this setting was postulated to be intrinsically unstable, via the so called "Marine Ice Sheet Instability" hypothesis (Hughes, 1973). This hypothesis is still up

2

for debate (Vaughan, 2008; Gudmundsson et al., 2012), while the trigger for the changes is thought to be enhanced ocean melting of the ice shelf (Dutrieux et al., 2014).

The dynamics of PIG are crucial for its future behaviour and therefore for its contribution to sea level rise. Due to the fast changes observed at PIG, a variety of modelling stud-
5 ies have been conducted. These studies address questions focusing on the sensitivity to changes in external conditions (ice shelf buttressing, basal conditions) (e.g. Schmeltz et al., 2002) and on the contribution to future sea level rise (e.g. Joughin et al., 2010). The over-arching question is, if the system will stabilise again in the near future, or if retreat might even accelerate (e.g. Katz and Worster, 2010; Gladstone et al., 2012; Favier et al., 2014;
10 Seroussi et al., 2014).

Ice flow models simulate the flow of glacier ice, which is due to a combination of internal deformation and basal motion. Depending on the subglacial setting, basal motion can dom-inate the overall motion of a glacier, which is also the case for large areas of PIG. Therefore, the basal sliding behaviour might be the crucial process to cause a further retreat or halt of
15 the system. Gudmundsson et al. (2012) show that stable grounding line positions can be found on a retrograde bed, using models with 2 horizontal dimensions. ~~We believe the~~ The basal sliding behaviour ~~is~~ could be a similarly important process as ~~is~~ the lateral buttressing.

The parametrisation of basal motion in ice flow models is ~~therefore~~ important for the overall dynamics of a glacier. On the other hand the difficulty of observing basal properties
20 renders the parametrisation one of the most challenging parts in ice flow modelling. In the absence of information on basal properties like bed type, structure and availability of liquid water, control methods are applied to simulate a complex glacier flow pattern, as present at PIG (e.g. MacAyeal, 1992; Joughin et al., 2009, 2010; Morlighem et al., 2010; Seroussi et al., 2014; Favier et al., 2014). These methods use the measured surface velocity field
25 to invert for basal properties or effective viscosity and to adjust basal sliding parameters. Depending on the focus of the study, these approaches can provide important insights into glacier dynamics.

The prognostic studies on PIG all use control methods to constrain basal sliding. Thus they define a spacially varying basal sliding parameter for the present flow state, and keep

it constant during the prognostic simulations. This way the basal sliding is somehow decoupled from the rest of the system. As the observable surface velocity field is a superposition of basal motion (sliding and bed deformation) and ice deformation, an inversion for basal sliding may introduce errors in the basal sliding that compensate for errors in deformational

5 part of the ice velocity. This is especially important for the strong temperature dependence of the flow rate factor used for the ice viscosity. In addition, the spatial distribution of a basal sliding parameter represents not only the flow state at a specific time of observation, but also the assumed thermal state in the model at the same time. One could imagine an area, that has significant sliding at the time of the inversion, could freeze on at later time steps,

10 but is allowed to slide at all times.

As the inversion for basal sliding parameters is not sufficient for the physical understanding of basal motion, we focus on basal sliding parametrisations that consider measured basal roughness distributions. This accessible bed information could be in further steps combined with for example a sufficient realistic and time-dependent hydrological model, to

15 consider changing basal conditions for the sliding behaviour of the glacier.

Here we present results of the thermo-mechanical 3D full-Stokes model COMice (implemented in the COMmercial finite element SOLver COMSOL Multiphysics©, cf. ~~Pattyn et al. (2013);~~ applied diagnostically to PIG. Initially we conduct a diagnostic inversion for a basal sliding parameter, as done in previous studies, to generate a reference simulation and analyse the

20 thermal structure of the glacier. In subsequent experiments we introduce two methods of connecting basal roughness measures to the parametrisation of basal sliding and therefore constrain basal sliding with more physically justified assumptions. Additionally, we couple the sliding behaviour to the basal temperature, adding another physically based constraint. The first method matches a single-parameter basal roughness measure for PIG, as pre-

25 sented in Rippin et al. (2011), onto a basal sliding parameter. The second method is based on ideas from Li et al. (2010), with a two-parameter basal roughness measure, which we apply to connect basal roughness to basal sliding.

4

2 The numerical flow model

2.1 Governing equations

The governing equations for the thermo-mechanical ice flow model COMice are the fluid dynamical balance equations, together with a formulation for the non-Newtonian rheology
5 of ice. The balance equations are set up for mass, momentum and energy, and solved for the velocity vector u, the pressure p and the temperature T.

The mass balance equation is given in case of incompressibility as

$$\text{div } u = 0. \tag{1}$$

The momentum balance equation is the Stokes equation, given by

10 $$\text{div } \sigma = -\rho_i g, \tag{2}$$

with the Cauchy stress tensor σ, the density of ice ρ_i and the acceleration of gravity $g = (0, 0, -g)^T$. The stress tensor σ is split into a velocity dependent part τ, the deviatoric stress, and a pressure dependent part pI, with the identity matrix I, such that $\sigma = \tau - pI$. For incompressible materials only the deviatoric stress τ can result in strains, and is thus
15 related to the velocity field u, via the strain-rate tensor $\dot{\varepsilon}$ and the effective viscosity μ, such that $\tau = 2\mu\dot{\varepsilon}$. The strain-rate tensor $\dot{\varepsilon}$ is given in components as

$$\dot{\varepsilon}_{ij} = \frac{1}{2}\left(\frac{\partial u_i}{\partial x_j} + \frac{\partial u_j}{\partial x_i}\right),$$

in relation to Cartesian basis vectors. The effective viscosity μ is described with use of Glen's flow law (Glen, 1955; Nye, 1957), such that

20 $$\mu(T', \dot{\varepsilon}_e) = \frac{1}{2}\left(A(T')\right)^{-1/n} \dot{\varepsilon}_e^{(1-n)/n}, \tag{3}$$

5

with the rate factor $A(T')$, the stress exponent n and the effective strain rate

$$\dot{\varepsilon}_e = \sqrt{\frac{1}{2} \mathrm{tr}(\dot{\varepsilon}^2)}, \tag{4}$$

which is the second invariant of the strain-rate tensor $\dot{\varepsilon}$. The homologous temperature T' is the temperature relative to the pressure melting point T_{pmp}, defined as

$$T' = T + \beta_c p, \tag{5}$$

with the Clausius-Clapeyron constant β_c. The pressure melting point T_{pmp} is described for typical pressures in ice sheets ($p \lesssim 50\,\mathrm{MPa}$) by a linear relation, such that

$$T_{\mathrm{pmp}} = T_0 - \beta_c p, \tag{6}$$

with the melting point at low pressures T_0. The rate factor $A(T')$ parametrises the influence of the temperature and the pressure onto the viscosity μ and is described by $A(T') = A_0 e^{-Q/RT'}$ (Greve and Blatter, 2009), with a pre-exponential constant A_0, the activation energy for creep Q and the gas constant R.

The energy balance equation is given as

$$\rho c_p(T) \left(\frac{\partial T}{\partial t} + \boldsymbol{u}\,\mathrm{grad}\,T \right) = \mathrm{div}(\kappa(T)\,\mathrm{grad}\,T) + \psi, \tag{7}$$

with the thermal conductivity $\kappa(T)$, the specific heat capacity $c_p(T)$ and an internal heat source term $\psi = 4\mu\dot{\varepsilon}_e^2$, which connects mechanical and thermal energy.

2.2 Boundary conditions

The balance equations are defined under the assumption that the thermodynamic fields are sufficiently smooth, thus continuously differentiable, which is only the case for the inner parts of the glacier. The outer boundaries need specifically formulated boundary conditions. The vertical boundaries are the upper surface z_s and the base z_b of the glacier. The lateral boundaries are given by the ice divide, an inflow area and the calving front. The grounding line indicates the change of the basal boundary conditions from grounded to floating ice.

2.2.1 ~~Mass~~Stokes flow

The upper surface can be seen to be traction free by assuming that wind stress and atmospheric pressure are negligible compared to the typical stresses in the ice sheet, such that $\boldsymbol{\sigma} \cdot \boldsymbol{n} = 0$.

5   Since the model is applied in a diagnostic manner and therefore the geometry is fixed, only the ice base needs a kinematic boundary condition, to prevent the flow to point into the ground, and is given as

$$\boldsymbol{u} \cdot \boldsymbol{n} = 0,$$

$\boldsymbol{u} \cdot \boldsymbol{n} = 0,$ with the unit normal vector $\boldsymbol{n}$ pointing outwards from the surface. This Dirichlet
10 condition is applied to the entire ice base, including grounded and floating parts, and also implies that no basal melting is considered.

2.2.2 ~~Stress~~

~~The upper surface can be seen to be traction free by assuming that wind stress and atmospheric pressure are negligible compared to the typical stresses in the ice sheet, such~~
15 ~~that $\boldsymbol{\sigma} \cdot \boldsymbol{n} = 0$.~~

At the base of the floating ice shelf shear stress induced by circulating sea water can be neglected (Weis et al., 1999) and the only stress onto the ice is exerted by hydrostatic water pressure. As the ice shelf floats it is assumed to fulfil the floating condition and the stress applied equals the stress of the displaced water column (Greve and Blatter, 2009),
20 such that

$$\boldsymbol{\sigma} \cdot \boldsymbol{n} = -p_{\text{sw}} \, \boldsymbol{n}, \tag{8}$$

with the water pressure p_{sw} defined as

$$p_{\text{sw}} = \begin{cases} 0 & \text{for} \quad z \geq z_{\text{sl}} \\ \rho_{\text{sw}} \, g \, (z_{\text{sl}} - z) & \text{for} \quad z < z_{\text{sl}}, \end{cases} \tag{9}$$

with the density of sea water ρ_{sw} and the mean sea level z_{sl}. Thus, the boundary conditions at the ice shelf base read

$$\boldsymbol{u} \cdot \boldsymbol{n} = 0 \quad, \quad (\boldsymbol{\sigma} \cdot \boldsymbol{n}) \cdot \boldsymbol{t}_x = 0 \quad \text{and} \quad (\boldsymbol{\sigma} \cdot \boldsymbol{n}) \cdot \boldsymbol{t}_y = 0, \tag{10}$$

with the unit tangential vectors $\boldsymbol{t}_x$ in the xz-plane and $\boldsymbol{t}_y$ in the yz-plane.

⁵   For the boundary condition of the grounded ice, it is assumed that the stress vector $\boldsymbol{\sigma} \cdot \boldsymbol{n}$ is continuous across the interface, such that $\boldsymbol{\sigma} \cdot \boldsymbol{n} = \boldsymbol{\sigma}_{\text{lith}} \cdot \boldsymbol{n}$, with the Cauchy stress tensor of the lithosphere $\boldsymbol{\sigma}_{\text{lith}}$. Since this tensor is not known, the condition has to be approximated. This is done with a sliding law that connects the basal sliding velocity $\boldsymbol{u}_{\text{b}} = (\boldsymbol{u} \cdot \boldsymbol{t}_x, \boldsymbol{u} \cdot \boldsymbol{t}_y)^T$, with the unit tangential vectors $\boldsymbol{t}_x$ in the xz-plane and $\boldsymbol{t}_y$ in the yz-plane, to the basal drag
¹⁰ $\boldsymbol{\tau}_{\text{b}} = ((\boldsymbol{\sigma} \cdot \boldsymbol{n}) \cdot \boldsymbol{t}_x, (\boldsymbol{\sigma} \cdot \boldsymbol{n}) \cdot \boldsymbol{t}_y)^T$.

So called "Weertman-type sliding laws" are commonly applied in ice flow modelling studies, for which the basis was established by Weertman (1957). He developed a mathematical description for the mechanisms that influence basal sliding. One focus lay hereby on connecting small scale processes with larger scale sliding effects. Nye (1969) and Kamb (1970)
¹⁵ worked on related problems and they all found that the basal sliding velocity $\boldsymbol{u}_{\text{b}}$ varies with some power of the basal shear stress $\boldsymbol{\tau}_{\text{b}}$, depending on the dominant mechanism. Additionally they find that the basal sliding velocity $\boldsymbol{u}_{\text{b}}$ also sensitively depends on the roughness of the bed.

The processes considered by Weertman (1957), Nye (1969) and Kamb (1970) are only
²⁰ relevant for sliding over hard bedrock, where an upper limit for sliding velocities is found ($\boldsymbol{u}_{\text{b}} < 20\,\text{m\,a}^{-1}$ (Cuffey and Paterson, 2010)). For faster sliding velocities weak deformable substrate or water filled cavities have to be present. Water filled cavities reduce the contact between the ice and the bedrock, therefore effectively reducing the roughness of the bed and their effect can be considered via the effective pressure $\boldsymbol{N}_{\text{b}} = -N_b \cdot \boldsymbol{n}$ (Bindschadler,
²⁵ 1983). Fast sliding velocities can only occur when the glacier base is at pressure melting point, but also below these temperatures some sliding can be present (Fowler, 1986). This mechanism can be reflected by a temperature function $f(T)$, which regulates sub-melt

sliding. Considering the above stated thoughts leads to a sliding law of the form

$$\boldsymbol{u}_{\mathsf{b}} = C_{\mathsf{b}}|\boldsymbol{\tau}_{\mathsf{b}}|^{p-1}N_{\mathsf{b}}^{-q}\, f(T)\, \boldsymbol{\tau}_{\mathsf{b}} = \frac{1}{\beta^2}\boldsymbol{\tau}_{\mathsf{b}}, \tag{11}$$

whereby C_{b} is originally seen as a roughness parameter, p and q are basal sliding exponents. When written in a linearised form, all effects influencing the basal sliding velocity $\boldsymbol{u}_{\mathsf{b}}$,
5 other than the linear relation to the basal shear stress $\boldsymbol{\tau}_{\mathsf{b}}$, are summerised in a basal sliding parameter β^2.

The overburden pressure of the ice is reduced in marine parts by the uplifting water pressure (Huybrechts, 1992), such that

$$N_{\mathsf{b}} = \left\{ \begin{array}{ll} \rho_{\mathsf{i}}gH & \text{for} \quad z_{\mathsf{b}} \geq z_{\mathsf{sl}} \\ \rho_{\mathsf{i}}gH + \rho_{\mathsf{sw}}g(z_{\mathsf{b}} - z_{\mathsf{sl}}) & \text{for} \quad z_{\mathsf{b}} < z_{\mathsf{sl}}, \end{array} \right. \tag{12}$$

10 with the ice thickness H. The assumptions made above imply that the base is perfectly connected to the ocean at any location in the domain that is below sea level. This assumption is plausible near the grounding line, but becomes highly speculative towards the marine regions further inland. An additional hydrological model would be needed to realistically simulate the effective basal pressure, but is beyond the scope of this study. Even though more
15 sophisticated parametrisations for the effective pressure exist (e.g. Leguy et al. (2014)), we stick with the strong assumption stated above, as water is likely present below all fast flowing parts of PIG (Smith et al., 2013), which coincide with the marine regions. Eq. 12 further implies, that the overburden pressure is cryostatic and neglects the dynamic contribution from the Stokes solution to the pressure. In general, the dynamic part is small compared
20 to the cryostatic part, even if the bed is rough or sliding is changing over short distances (Pattyn et al., 2008, supplementary material).

The temperature function $f(T)$ is taken as suggested by Budd and Jenssen (1987) as an exponential function, such that

$$f(T) = e^{\nu(T - T_{\mathsf{pmp}})}, \tag{13}$$

9

with a submelt sliding parameter ν.

The dynamic boundary condition at the base is implemented consisting of a tangential part (Eq. 11) and a normal part (Eq. 12) such that

$$\boldsymbol{\sigma} \cdot = \beta^2 u_{\mathsf{b}x} + \beta^2 v_{\mathsf{b}y} - N_{\mathsf{b}}. \quad \boldsymbol{u} \cdot \boldsymbol{n} = 0 \quad , \quad (\boldsymbol{\sigma} \cdot \boldsymbol{n}) \cdot \boldsymbol{t}_x = \beta^2 \boldsymbol{u} \cdot \boldsymbol{t}_x \quad \text{and} \quad (\boldsymbol{\sigma} \cdot \boldsymbol{n}) \cdot \boldsymbol{t}_y = \beta^2 \boldsymbol{u} \cdot \boldsymbol{t}_y.$$
(14)

5   ~~This~~ The stress boundary condition is a Robin boundary condition as it depends on the velocity and the velocity gradients. With $\beta^2 = 0$ for the floating part, this boundary condition equals Eq. 10.

Ice divides can be seen as mirror points where the direction of the driving stress and flow on one side of the divide opposes that of the other side. No flow across the ice divide is
10 allowed, the tangential stresses vanish and therefore the boundary condition for ice divides is given by

$$\boldsymbol{u} \cdot \boldsymbol{n} = 0 \quad , \quad (\boldsymbol{\sigma} \cdot \boldsymbol{n}) \cdot \boldsymbol{t}_x = 0 \quad \text{and} \quad (\boldsymbol{\sigma} \cdot \boldsymbol{n}) \cdot \boldsymbol{t}_y = 0. \quad \boldsymbol{u} \cdot \boldsymbol{n} = 0 \quad , \quad (\boldsymbol{\sigma} \cdot \boldsymbol{n}) \cdot \boldsymbol{t}_x = 0 \quad \text{and} \quad (\boldsymbol{\sigma} \cdot \boldsymbol{n}}$$
(15)

with the unit normal vector $\boldsymbol{n}$ pointing outwards from the surface and lying in the xy-plane.

The boundary condition at the vertical calving front is given by Eq. 8 and Eq. 9, where the
15 normal vector is pointing towards the ocean and lies in the xy-plane. For the inflow region a Dirichlet condition prescribes an inflow velocity field calculated analytically with the Shallow Ice Approximation (Hutter, 1983; Morland, 1984). To the outer wall of the ice rises a no slip condition is assigned, as they are implemented as holes in the geometry.

2.2.2 Temperature

20 The boundary conditions for the upper surface is given by Dirichlet conditions in prescribing the average annual surface temperature $T_{\mathsf{s}}(x,y,t)$. At the base of the grounded ice two

10

cases are to be distinguished. For a cold base, that is, a basal temperature below the pressure melting point, the boundary condition has to be formulated as a Neumann condition and the temperature gradient is prescribed as

$$\operatorname{grad} T \cdot \boldsymbol{n} = \frac{q_{\text{geo}} + q_{\text{fric}}}{\kappa(T)}, \tag{16}$$

5 with the geothermal flux q_{geo} and the friction heating due to basal sliding $q_{\text{fric}} = \boldsymbol{u}_{\text{b}} \cdot \boldsymbol{\tau}_{\text{b}}$ (Pattyn, 2003). If the basal temperature reaches the pressure melting point in the grounded part or the freezing temperature of seawater T_{sw} in the floating part, it has to be switched to a Dirichlet condition

$$T = \begin{cases} T_{\text{pmp}} & \text{if grounded,} \\ T_{\text{sw}} & \text{if floating.} \end{cases} \tag{17}$$

10 The boundary condition for the ice divide and the calving front are based on the assumption that there is no temperature gradient across the surface. It can thus be written in form of a thermal insulation $(\kappa(T) \operatorname{grad} T) \cdot \boldsymbol{n} = 0$. Lastly, temperatures at the inflow boundary are prescribed by a linear profile $T_{\text{lin}} = \frac{T_{\text{pmp}} - T_{\text{s}}}{z_{\text{s}} - z_{\text{b}}}(z_{\text{s}} - z) + T_{\text{s}}$.

2.3 Implementation

15 The thermo-mechanically coupled 3D full-Stokes model COMice is implemented in the COMmercial finite element SOLver COMSOL Multiphysics® (cf. Wilkens (2014) for implementation details). The model has been successfully applied in the diagnostic tests in the MISMIP 3D model intercomparison project (Pattyn et al., 2013) and the ISMIP-HOM experiments (Pattyn et al., 2008). The ice flow model solves for the the velocity vector $\boldsymbol{u}$, the

20 pressure p and the temperature T. The unstabilized Stokes equation (Eq. 2) is subject to the Babuska-Brezzi condition, which states that the basis functions for p ~~are~~ have to be of lower order than for $\boldsymbol{u}$. Therefore we use linear elements for p and quadratic elements for $\boldsymbol{u}$ (P1+P2). The energy balance equation Eq. 7 is discretized with linear elements. To avoid

11

numerical instabilities due to strong temperature advection, and thus to ensure that the element Péclet number is always < 1, we use consistent stabilization methods provided by COMSOL. Eq. 7 is solved using a Galerkin Least Square (GLS) formulation (Codina, 1998) in streamline direction and crosswind diffusion (Hauke and Hughes, 1998) orthogonal to

[5] the streamline direction. The chosen stabilization methods add less numerical diffusion the closer the numerical solution comes to the exact solution.

To the effective strain rate $\dot{\varepsilon}_e$ (Eq. 4) a small value of $10^{-30}\,\text{s}^{-1}$ is added, to keep the term non-zero. Model experiments have shown, that this does not affect the overall results (Pattyn, 2003; Cornford et al., 2012). The scalar values for all parameters used throughout

[10] this study are listed in Tab. 1.

All Dirichlet boundary conditions are implemented as a weak constraint~~that means the constraint is~~, which means that constraints are enforced in a local average sense. This gives a smoother result than the standard method in COMSOL where constraints are enforced pointwise at node points in the mesh. The Neumann condition (Eq.16) together with

[15] the Dirichlet condition for the basal temperature at the base (Eg. 17) is implemented in a way, that a switch between these two types is avoided. This ~~due to the fact that~~ is done because a jump from T_{pmp} to T_{sw} in the area of the grounding line lead to non-convergence of the flow model. Therefore, a heat flux is prescribed, as long as $T < (T_{\text{b,max}} - 0.01)$. The expression $T_{\text{b,max}}$ prescribes a spacially variable field that defines the maximal basal

[20] temperature allowed for a region (T_{pmp} for grounded areas, T_{sw} for floating areas). If $T \geq (T_{\text{b,max}} - 0.01)$, the heat flux is gradually reduced and turns zero when $T = (T_{\text{b,max}} + 0.01)$. This procedure ensures that the basal heat flux can not increase T_{b} above $T_{\text{b,max}} + 0.01$. The smoothing of the step function ensures numerical stability, which was not found with a sharp step. The implementation is similar as in Aschwanden and Blatter (2009).

[25] ### 2.3.1 Mesh

To maximise the resolution while minimising the amount of elements, we use an unstructured finite element mesh. The upper surface is meshed first with triangles. The horizontal edge lengths are $5 - 500\,\text{m}$ at the grounding line and the calving front, $50 - 1000\,\text{m}$ at the

12

inflow area and $100 - 2000\,\text{m}$ at the rest of the outer boundary. The resulting 2D surface mesh is extruded through the glacier geometry with a total of 12 vertical layers everywhere. The thickness of the vertical layers varies only with ice thickness. The spacing between the layers is refined towards the base. The ratio of the lowest to the upper most layer thickness

5 is 0.01, leading to a thickness of the lowest layer of about $5\,\text{m}$ for a total ice thickness of $3000\,\text{m}$. The final mesh consists of $\sim 3.5 \times 10^5$ prism elements, which results in $\sim 5 \times 10^6$ degrees of freedom (DOF), when solved for all variables.

2.3.2 Solver

For solving the nonlinear system, a direct segregated solver is used, which conducts a

10 quasi-Newton iteration. It solves consecutively: first for the velocity $\boldsymbol{u}$ and the pressure p, and thereafter for the temperature T (COMSOL, 2012). This allows for reduced working memory usage. For the remaining linear systems of equations the direct solver Pardiso (COMSOL (2012) and http://www.pardiso-project.org/, last access: 9 December 2014) is applied. While uncommon for such large numbers of DOF's, it proved to be computationally

15 viable and robust.

3 Data

3.1 Geometry

The geometry of the model was built with a consistent set of surface elevation, ice thickness and bed topography on a $1\,\text{km}$ grid, created by A. Le Brocq and kindly provided by her for

20 this work. The data set represents the thickness distribution of PIG for the year 2005 and earlier. The Le Brocq data are based on the surface elevation data of Bamber et al. (2009) and the ice thickness data of Vaughan et al. (2006). The grounding line position used is given by a combination of the positions in the MODIS Mosaic Of Antarctica (MOA, Bohlander and Scambos, 2007), corresponding to the years 2003/2004, the position in Rignot

25 (1998), corresponding to 1996, and the position that gives the smoothest ice thickness join

13

of the glacier geometry, assuming the floatation condition. The model domain and grounding line is indicated in Fig. 1. The location of the ice rises pinning the ice shelf at present are detected on TerraSAR-X images from 2011, with assistance of interferograms from Rignot (2002). Please note that ice rises are not indicated in Fig. 1.

3.2 Ice flow velocity

The observed surface velocity is taken from Rignot et al. (2011), shown in Fig. 1, and used to validate the reference simulation. The numbering of the tributaries 1-10 feeding the central stream is based on Stenoien and Bentley (2000). The numbering used in Vaughan et al. (2006), Karlsson et al. (2009) and Rippin et al. (2011) is the same for the even numbers, but shifted by 1 for the odd numbers, as they missed tributary 1 from the numbering by Stenoien and Bentley (2000). We extended the numbering from Stenoien and Bentley (2000) to the tributaries 11-14, which are entering the ice shelf. Finally, Fig. 1 indicates the locations of the different types of lateral boundaries (ice divide, inflow and calving front).

3.3 Temperature

The surface temperature used here is on a 5 km grid compiled by Le Brocq et al. (2010) (ALBMAP v1), based on the temperature data described in Comiso (2000). We use the geothermal flux q_{geo} from Purucker (2012, updated version of Fox Maule et al. (2005)), because a variety of sensitivity tests showed, that other data sets lead to too high velocities in regions with no or little basal sliding.

3.4 Roughness

In this study we use two different measurements of basal roughness beneath the PIG. The first one is ~~a~~ the single-parameter roughness measure as presented in Rippin et al. (2011) (c.f. Fig. 4b therein) and represents the methodology often employed to define subglacial roughness (Hubbard et al., 2000; Taylor et al., 2004; Siegert et al., 2004, 2005; Bingham and Siegert, 2007; Bingham et al., 2007; Rippin et al., 2011). This usual approach effec-

14

tively provides a measure of bed obstacle amplitude or vertical roughness. The second measure, which we calculate for this study, follows the work of Li et al. (2010) and Wright et al. (2012), and more recently Rippin et al. (2014)~~who~~. They introduce a second parameter which effectively provides a further measure ~~, but this time~~ of the frequency or wave-

5 length of roughness obstacles (Rippin et al., 2014). Both roughness measures are based on Fast Fourier transforms (FFTs). ~~An FT~~ FFT can be used to transform any surface into a sum of several periodically undulated surfaces. In a number of recent glaciological studies, ~~these data are~~ basal topography data is transformed into a single-parameter roughness measure (ξ) which is defined as the integral of the spectrum within a specified wavelength

10 interval. This method represents the amplitude of the undulations, but information about the frequency is lost. For PIG the single-parameter roughness measure ξ was calculated by Rippin et al. (2011) from a RES data set generated in austral summer 2004/05 (Vaughan et al., 2006). It is the same data set the model geometry is based on (Sect. 3), still the roughness measure includes higher resolution information, as the derivation is based on

15 along track sample spacing of the order of 30 m (cf. Rippin et al. (2011)). Both data sets are then gridded with 1 km spacing.

~~In~~ By applying the work of Li et al. (2010), we introduce a second parameter so that as well as being able to represent the amplitude (ξ) we are also able to explore the frequency (η) of the undulations. This measure is calculated as the total roughness divided by the bed

20 slope roughness (Rippin et al., 2014). Li et al. (2010) provide guidance ~~as to~~ on how to interpret these two parameters in terms of their different basal topographies, along with their geomorphic implications. The interpretation from Li et al. (2010) is based on ideas by Bingham and Siegert (2009), which give an interpretation for the single-parameter roughness. Rippin et al. (2014) extended the interpretation for the two-parameter roughness measure.

25 The implications for PIG will be discussed below.

Because of the statistical meanings of ξ and η, they can be used as representatives for the vertical and horizontal length scales present at the base. To do so the integration interval for $\{\xi, \eta\}$ should be in the metre-scale waveband (Li et al., 2010). The two-parameter roughness measure for PIG was calculated for this study. The spatial resolution of the un-

derlain data for PIG is 34 m. A moving window is calculated with $N = 5$ ($2^N = 32$), which is the minimum for N that should be used (e.g. Taylor et al., 2004). With a spatial resolution of 34 m this leads to a moving window length of 1088 m, which is in the metre-scale waveband required by Li et al. (2010), to be able to apply the data in a sliding relation.

5   The received fields of ξ and η for PIG are shown in Fig. 2. According to Li et al. (2010), different basal properties and related geomorphic implications can be distinguished from patterns of ξ and η. A marine setting with intensive deposition and fast and warm ice flow, as proposed for the central part of PIG, is characterised by low values of ξ and high values of η, thus low-amplitude, low-frequency roughness. Here it has to be noted that the

10   second parameter η should be more accurately seen as representing the wavelength of roughness, rather than the frequency, as high values correspond to low frequencies (Rippin et al., 2014). Nonetheless we continue here refering to η as the roughness frequency for consistency with Li et al. (2010). The suspected low-amplitude, low-frequency roughness is not necessarily found in the central trunk area, as can be seen in Fig. 2. Instead it seems

15   to be more dominated by low-amplitude, high-frequency roughness, which can, following Li et al. (2010), be interpreted as a continental setting after intensive erosion, also with fast and warm ice flow. Still, this interpretation can not be seen as a contradiction to the suspicion of the presence of marine sediments. It is important to state that absolute values of roughness cannot be derived from these calculations~~, but rather the patterns~~. It is rather

20   the pattern relating to relative roughness values that ~~are~~ is significant.

4   Experiment description

4.1   Experiment 1: Reference Simulation

The main difficulty is to capture the distinct surface flow pattern, by making appropriate assumptions about the basal sliding behaviour. Many ice modelling studies use a constant

25   set of basal sliding parameters to reproduce somewhat realistic surface velocity fields (e.g. Rückamp, 2011; Kleiner and Humbert, 2014). This approach can not be adopted for PIG,

as it leads to a shut down of parts of the fast flowing main trunk, due to very low basal shear stresses in that region (Joughin et al., 2009; Morlighem et al., 2010). Instead, for our reference simulation, an inversion for basal parameters is conducted. This approach will lead to a realistic reproduction of the surface flow velocity field and lets us analyse the
5   thermal structure of the glacier.

The inversion method (cf. Schmeltz et al., 2002) used for our reference simulation starts by assuming the linearized form of Eq. 11, thus $\tau_b = \beta^2 u_b$, with β^2 being the basal sliding parameter to be inferred. Additionally a simulation is conducted, where the glacier base is not allowed to slide. Therefore the resulting surface velocity field $u_{s,nosl}$ can be seen to
10   be solely due to internal deformation. The basal sliding velocity u_b can be approximated by subtracting the surface velocity due to internal deformation $u_{s,nosl}$ from the measured surface velocity field u_{obs} (Rignot et al. (2011), Fig. 1). The basal drag from the simulation where no basal sliding is allowed $\tau_{b,nosl}$ is taken as a good first representative of the real basal drag distribution τ_b. With this the field of the basal sliding parameter β^2 is defined as

15   $$\beta^2 = |\tau_{b,nosl}| (|u_{obs}| - |u_{s,nosl}|)^{-1}, \tag{18}$$

shown in Fig. 3. This is a significant different approach as in e.g. Joughin et al. (2009), Morlighem et al. (2010) and Seroussi et al. (2014) where they minimize a cost function.

The basal sliding parameter β^2 is subsequently applied in the forward model in the linear sliding law. Since the amount of internal deformation in the ice crucially depends on the ice
20   temperature (Eq. 3), it is important to consider a realistic temperature distribution within the ice. At this point it is important to note, that the model is applied in a diagnostic manner and therefore the received temperature distribution is a steady state one for a fixed geometry with constant boundary conditions, which might differ from the actual transient field. Nonetheless the received field is likely to show a better approximation to reality than simply
25   assuming a certain distribution. To consider a realistic temperature distribution within the ice, we conduct the above described procedure in an iterative manner. We first conduct a "no sliding" simulation `nosl,1`, with a constant temperature of $T = 263.15\,\text{K}$. The resulting surface velocity field $u_{s,nosl,1}$ and basal drag $\tau_{b,nosl,1}$ lead to a basal sliding parameter β_1^2.

This basal sliding parameter enters a next simulation step where basal sliding sl,1 is accounted for and the temperature field is solved for. The temperature distribution enters the next "no sliding" simulation nosl,2 as a constant field. Again a basal sliding parameter is found, entering the next simulation step sl,2, which is our final reference simulation
5 ref. Thus the procedure is stopped after two iterations, and listed in a schematic manner as: nosl,1($T = 263.15$ K) $\rightarrow \beta_1^2 \rightarrow$ sl,1(T solved) $\rightarrow$ nosl,2(T from sl,1) $\rightarrow \beta_2^2 \rightarrow$ sl,2/ref(T solved).

The reference simulation serves as validation parameter for the subsequent experiments. As a quantitative measure the root-mean-square (RMS) deviation RMS$_{u_s}$ (unit: m a^{-1}) be-
10 tween the simulated surface velocity field $u_{s,sim}$ and the reference surface velocity field $u_{s,ref}$ is given by

$$\text{RMS}_{u_s} = \sqrt{\frac{1}{m} \sum_{i=1}^{m} (||u_{s,sim}|_i - |u_{s,ref}|_i|)^2}, \tag{19}$$

with m being the number of discrete values on a regular grid with 1 km spacing. The comparison is done in three distinct regions: fast flow velocities ("Fast"), slower flow velocities
15 ("Slow") and the entire model region ("All") (detailed description in Wilkens (2014)). The regions of all tributaries (1-14), the central stream (CS) and the shelf area (Shelf) are combined to the region "Fast", while the remainder is the region "Slow" (cf. Fig. 8b and 8c)

4.2 Experiment 2: Parametrisation with single-parameter roughness

The approach in the reference simulation is dissatisfying when aiming to constrain basal
20 sliding with physical parameters at the base of the glacier. Therefore, we introduce in this experiment a parametrisation of basal sliding that ~~consider~~ considers the basal roughness below the glacier in the formulation of the commonly used Weertman-type sliding law (Eq. 11), with the aim to reproduce the surface velocity field of PIG. Instead of inverting for one spatially varying parameter, we now connect the basal sliding parameter C_b to the measured

18

single-parameter roughness measure ξ (Rippin et al., 2011), Sect. 3.4, as it is closest to the ~~originally~~ original physical meaning of C_b.

The absolute values of the roughness measure ξ are dependent on parameters chosen for its derivation (e.g. wavelength interval in Rippin et al., 2011). At the same time the sliding
5 parameter C_b depends not only on mechanical properties, such as basal roughness, but also thermal properties. Therefore, the roughness measure ξ can not directly be used as the sliding parameter. To use the roughness information, we select a range for the sliding parameter C_b, obtained via the approximation

$$C_b = \frac{\left(|\boldsymbol{u}_{\text{obs}}| - |\boldsymbol{u}_{\text{s,nosl}}|\right) N_b^q}{|\boldsymbol{\tau}_{\text{b,nosl}}|^p}. \tag{20}$$

10 To obtain a roughness parameter that depends on the roughness measure ξ, the resulting range $[C_{\text{b,min}}, C_{\text{b,max}}]$ is mapped onto the range of the roughness measure $[\xi_{\text{min}}, \xi_{\text{max}}]$, such that

$$C_b(\xi) = \frac{(C_{\text{b,max}} - C_{\text{b,min}}) \cdot (\xi - \xi_{\text{min}})}{(\xi_{\text{min}} - \xi_{\text{max}})} + C_{\text{b,max}}. \tag{21}$$

The lowest roughness correlates with highest basal sliding and therefore highest values of
15 ~~C_ξ~~$C_b(\xi)$. In the following we will refer to the basal sliding parameter $C_b(\xi)$, when it is related to the basal roughness measure ξ, as C_ξ.

In total we conduct 15 simulations for experiment 2, where each parameter combination represents a potential subglacial setting. In all simulations the coefficient $p = 1$ is kept constant, while q is varied to investigate the effect of the effective pressure onto the sliding ve-
20 locities ($q \in \{0, 1, 2\}$). This results in varying minimum and maximum values for C_ξ for each parameter combination. To account for potential outliers in the C_ξ distribution, we have subsequently narrowed the range of C_ξ. This results in varying minimum and maximum values for C_ξ for each parameter combination. Hence, simulations with an identifier 1-5 are conducted with $q = 0$ and 5 different ranges of C_ξ, simulations 6-10 with $q = 1$ and 5 different
25 ranges of C_ξ and simulations 11-15 with $q = 2$ and 5 different ranges of C_ξ. The ranges of C_ξ can be found in ~~(Tab. 5.2 Wilkens, 2014) .~~Tab. 5.2 in Wilkens (2014).

4.3 Experiment 3: Parametrisation with two-parameter roughness

The aim of this experiment is to test the idea of Li et al. (2010) for its applicability to PIG. This approach also relates the basal roughness to the basal sliding velocity~~but~~. This time the roughness is represented by a two-parameter roughness measure for the amplitude ξ and frequency η of the undulations. The approach is based on Weertmans original formulation (Weertman, 1957) of describing the sliding mechanisms of regelation and enhanced creep, such that

$$\boldsymbol{u}_{\mathsf{b}} = C_{\mathsf{W}} \left(\boldsymbol{\tau}_{\mathsf{b}} \frac{l^2}{a^2} \right)^{\frac{(1+n)}{2}}, \tag{22}$$

whereby C_{W} is a parameter defined by thermal and mechanical properties of the ice, l is the obstacle spacing, a the obstacle size (cf. Weertman (1957)) and $n = 3$ the stress exponent.

Li et al. (2010) state that the two-parameter roughness measures ξ and η, representing the amplitude and frequency of the roughness (cf. Sect. 3.4), can be used as a proxy for the vertical and horizontal length scales present at the base, due to their statistical meanings, such that $a = c_1\sqrt{\xi}$ and $l = c_2\sqrt{\eta}$, with c_1 and c_2 being proportionality factors.

Entering this into Weertmans original formulation (Eq. 22) and additionally including a temperature function $f(T)$ as introduced above, leads to

$$\boldsymbol{u}_{\mathsf{b}} = C_{\mathsf{L}} f(T) \left(\boldsymbol{\tau}_{\mathsf{b}} \frac{\eta}{\xi} \right)^{\frac{(n+1)}{2}}, \tag{23}$$

with the constant $C_{\mathsf{L}} = C_{\mathsf{W}}(c_2/c_1)^{1+n}$. As the proportionality factors c_1 and c_2 are not further defined, we take C_{L} as a single parameter to adjust.

~~To estimate an~~ The upper and lower ~~bound~~ bounds for C_{L} ~~the reference simulation is used to derive the spatial variability of C_{L} from Eq. 23 as:~~ are obtained via

$$C_{\mathsf{L}} = \left(|\boldsymbol{u}_{\mathsf{obs}}| - |\boldsymbol{u}_{\mathsf{s,nosl}}| \right) |\boldsymbol{\tau}_{\mathsf{b,nosl}}|^{-\frac{(n+1)}{2}} \left(\frac{\xi}{\eta} \right)^{\frac{(n+1)}{2}}. \tag{24}$$

20

The vast majority of the values lie within $C_L = [3 \times 10^{-2}; 3 \times 10^2]$ Pa^{-2} m a^{-1}. We conduct 18 simulations for this experiment, whereby the value of C_L (Eq. 23) is varied in this range.

For all simulations conducted for experiment 3, only Eq. 2 is solved for, due to time constraints (cf. Wilkens (2014)). The temperature distribution within the ice is taken from the reference simulation. Use of the temperature field from the reference simulation gives the opportunity to connect the sliding behaviour to the basal temperature, thus only allowing ice to slide where T is close to T_{pmp}.

5 Results

5.1 Experiment 1

The resulting surface velocity field from the reference simulation is shown in Fig. 4. The general pattern of the surface velocity field is well reproduced in the reference simulation, compared to the observed surface velocity field (Fig. 1). The tributaries are all in the right location and the velocity magnitudes agree in most areas well. The highest differences between $|\boldsymbol{u}_{\text{s,ref}}|$ and $|\boldsymbol{u}_{\text{obs}}|$ are found in the ice shelf, where the simulated velocities are up to 1 km a^{-1} smaller than the observed ones.

When solely looking at the velocity magnitudes we again find that for higher velocities the simulated velocity field is lower than the observed field (Fig. 5). The spread around the diagonal for lower velocities appears bigger, which is mainly due to the logarithmic axes chosen. For higher flow velocities the direction of flow of the simulated field agrees well to the direction of the observed field. This is shown as a colour code for the angle offset between the velocity vectors in Fig. 5. For slower velocities the angle offset is bigger, coinciding with a higher measurement error for slower velocities.

The ~~simulations~~ simulation shows, that under PIG large areas are temperate (Fig. 6). In general the overall flow pattern is reflected in the basal temperature structure, with fast flowing areas being underlain by a temperate base. Fig. 7 shows the homologous temperature T'_{ref} at three vertical slices, of which the ~~location is~~ locations are indicated in Fig. 6.

21

The slice located furthest away from the ice shelf ~~show~~ shows that the base is mainly temperate, while the inner ice body (away from the base) is predominantly cold (Fig. 7a). A similar picture is found in the next slice which is located further downstream towards the ice shelf (Fig. 7b). Here, additionally a cold core can be seen, located in the fast flowing central 5 stream.

The next slice partly crosses the ice shelf (Fig. 7c). It can be well observed that a cold core is entering the ice shelf. In the vicinity of tributary 11 (cf. Fig. 1) a small temperate layer is found.

5.2 Experiment 2

10 First of all we show in Fig. 8a the RMS_{u_s} deviations between the reference simulation and experiment 2 for all 15 conducted parameter combinations. It can be seen, that the "Fast" regions differ most for all parameter combinations tested here. Additionally for the entire region "All" there seems to be no single parameter combination, that minimises the RMS_{u_s} value. Although the RMS is relatively high some of the complex surface flow features could 15 be reproduced with our approach, which can only be seen by looking at the qualitative structure of the resulting surface flow fields. Fig. 8b shows the surface velocity field with $q = 0$, that means the effect of the effective pressure is cancelled out (simulation identifier 2). The location of tributary 7 (and slightly 11) and the central stream are well reproduced.

Although the central stream is in general well reproduced, the inflow into the ice shelf is 20 characterized ~~with~~ by a drop of flow velocities, which does not coincide with the observed velocities. In the simulations where the effective pressure in considered with $q = 2$ (simulation identifiers 11-15), a much better representation of the central stream at the inflow into the ice shelf across the grounding line is found, as can be seen for example in the surface flow field from simulation 11, shown in Fig. 8c. The influence of the effective pressure N_b is 25 thus emphasised. At the same time this method does not lead to a full reproduction of the surface flow structure. This suggests that other processes, not considered here, may also be important for the basal sliding behaviour. A possibility, not tested yet due to cpu time constraints (for a detailed description of the solution time of the simulations refer to Wilkens

(2014)), is the effect of the basal stress exponent p. Increasing it would possibly to some extend regulate the high velocities in some areas, due to low basal stresses.

The basal homologous temperature from simulation 2 (Fig. 9) shows a very clear structure of the temperate base below the tributaries, even though they are not clearly visible in
5 the flow field (cf. Fig. 8b). The temperature driven separation between tributaries 2 and 4 and tributaries 7 and 9 are even better visible than in the reference simulation (cf. Fig. 6). The structure of the basal homologous temperature of all other simulations look very similar to that of simulation 2, ~~although~~ but the total area fraction of ice at pressure melting point varies, as well as the separation between the tributaries.

10 Another interesting feature found in the structure of the basal temperature from simulation 2 is the advection of warmer ice into the shelf. This feature can be attributed to the implementation of the thermal basal boundary condition in the shelf ~~.~~ (cf. Sect. 2.3). While the heat flux is not allowed to raise the temperature above $271.15\,\mathrm{K}$, it does not hinder the advection of warmer ice from the grounded areas. The structure of the bands of warmer ice
15 agree well with melt channels below the ice shelf as found by Vaughan et al. (2012).

5.3 Experiment 3

The $\mathrm{RMS}_{\boldsymbol{u}_\mathrm{s}}$ deviations between the reference simulation and and all conducted parameter combinations in experiment 3 show a somewhat regular pattern (Fig. 10a). For the slower flowing areas, the $\mathrm{RMS}_{\boldsymbol{u}_\mathrm{s}}$ value increases with increasing C_L. For the faster flowing areas,
20 the $\mathrm{RMS}_{\boldsymbol{u}_\mathrm{s}}$ value first slightly decreases with increasing C_L, and, after reaching a minimum of $\mathrm{RMS}_{\boldsymbol{u}_\mathrm{s}} = 500\,\mathrm{m\,a^{-1}}$ for $C_\mathrm{L} = 1.58\,\mathrm{Pa^{-2}\,m\,a^{-1}}$, increases with increasing C_L. Since we conduct simulations with discrete values for C_L, the value of $\mathrm{RMS}_{\boldsymbol{u}_\mathrm{s}} = 500\,\mathrm{m\,a^{-1}}$ represents the minimum value for the simulations conducted here, and not an absolute minimum. The $\mathrm{RMS}_{\boldsymbol{u}_\mathrm{s}}$ value for the entire region "All", shows a similar behaviour of first decreasing and
25 then increasing with increasing C_L, with a minimum $\mathrm{RMS}_{\boldsymbol{u}_\mathrm{s}}$ value of $271\,\mathrm{m\,a^{-1}}$ for $C_\mathrm{L} = 1\,\mathrm{Pa^{-2}\,m\,a^{-1}}$.

Although RMS values reveal a slight minimum, the surface velocity field of PIG is not reproduced with all its features. For higher C_L values, that reproduce the velocities in the

central stream in a better manner, the velocities in the slower flowing area around tributaries 3, 5, 7 and 9, located to the South of the main stream, are simulated much too high.

A striking feature of all simulations is, that the central stream is partitioned into a faster flowing upper part, and a slower flowing lower part in the vicinity of the ice shelf. We show that exemplarily for a C_L value with a low RMS value and a C_L value with a high RMS value (Fig. 10b and 10c). However, when looking at the structure of the surface flow fields it is apparent that some features of the observed surface flow field are reproduced.

Additionally, the area around tributary 14 behaves slightly different to most other tributaries. It speeds up much faster for much lower values of C_L. This is related to the low roughness measures ξ and η in that region.

6 Discussion

We have shown that the complex surface flow structure of PIG could be well reproduced with our simplified approach of an inversion for a basal sliding parameter β^2 in the reference simulation. Although the simulated flow pattern agrees well with observations, some differences in the magnitude of the surface flow velocities to observations were found. These differences are highest in the ice shelf, and might be partly related to a slower inflow from the grounded areas where the difference is about $1\,\mathrm{km\,a^{-1}}$. This might be due to the position of the grounding line in our model which is further downstream than the location in 2009, to which the observed surface velocity field belongs (2007–2009). As we run the flow model in diagnostic manner without a relaxation of the geometry, the simulated ice flow could not be consistent with the geometry. Or it might be caused by the simplified method of inferring β^2, as $\tau_{\mathrm{b,nosl}}$ is not vanishing near the grounding line, as would be expected (cf. Joughin et al. (2010) and Morlighem et al. (2010)).

However, the main cause though seems to be that we did not account for the highly rifted shear margins. These shear margins have been shown to be rheologically softer than undamaged ice (e.g. Humbert et al., 2009). In reality the shear margins partly uncouple the fast flowing central part from the surrounding ice. In our study we neglect the effect

24

of shear margins and treat them rheologically equal to undamaged ice. This leads to an overestimation of the flow outside the central stream, and an underestimation within the central stream in the main trunk. The softening due to shear margins can be included in different ways, as for example done in Joughin et al. (2010); Favier et al. (2014).

From the simulated temperature distribution, we found that the base of the glacier is predominantly temperate with the absence of a significant temperate layer; the rest of the inner ice body is mainly cold. This finding is consistent with the general definition of an Antarctic glacier, where, due to cold conditions at the surface, the cold-temperate transition surface (CTS) (Blatter and Hutter, 1991) is located at or near the base. To form a significant basal temperate layer Blatter and Hutter (1991) state that strain heating is the necessary mechanism. This also agrees well with our results, as the flow of PIG is dominated by basal sliding and therefore strain heating due to internal deformation is small. Only an area around tributary 11 (cf. Fig. 6 and 7c), where strain heating is much higher, shows the existence of a somewhat larger temperate layer at the base. Unfortunately there are no measured (deep) ice core temperatures available at PIG, to which our results could be compared. Nonetheless our findings of a temperate base below some parts of PIG are supported by findings from Smith et al. (2013), who find hints for the existence of water below the glacier.

As the first new parametrisation for basal sliding we tested the applicability of including actual measured roughness data in the commonly used Weertman-type sliding law. The new parameter C_ξ is applied in the basal sliding law and we were able to reproduce many of the tributaries although not the full complexity of the flow structure. For instance, the central stream is in large areas underlain by a very smooth bed, indicated by a low roughness measure ξ, which becomes rougher towards the grounding line.

We have shown, that the influence of the effective pressure onto basal sliding must be large close to the grounding line to keep the flow velocities high. As part of the overburden pressure is supported by the basal water of the marine setting of the glacier, the effective pressure is low and basal motion is therefore facilitated.

The locations of the fast flowing tributaries and the central stream are well indicated by a temperate base. The structure is visible even more clearly than for the reference simu-

lation. This supports the idea that the location of some tributaries is influenced by basal temperatures.

A full reproduction of the surface flow structure is not achieved with the single-parameter roughness measure. This suggests that other processes, not considered here, are also important for the basal sliding behaviour. In addition, the basal stress exponent p would to some extend perhaps regulate the high velocities in some areas, due to low basal stresses. The effect of p on the flow field has not been investigated here, but should be considered in the future.

For the second new parametrisation for basal sliding we test the applicability of a theory developed by Li et al. (2010) to the region of PIG, that connects a two-parameter roughness measure $\{\xi, \eta\}$ to the basal sliding law. This approach additionally accounts for the frequency of roughness but neglects the effective pressure. The results of the surface flow field show, that the central stream in all the simulations from this experiment is partitioned into a faster flowing upper part, and a slower flowing lower part, in the vicinity of the ice shelf. No single value for C_L could be found, that reproduces the surface velocity field of PIG with all its features. To account for the frequency roughness does not lead to an overall better representation of the flow compared to the single-parameter approach. We expect that if the effective pressure at the base is considered in the sliding formulation of Li et al. (2010), the results would significantly improve as the reduced effective pressure at the grounding line in the marine setting of PIG would favour higher sliding velocities.

Despite the inability of a complete reproduction of the surface flow field of PIG with the methods using the roughness measure, this approach represents some important flow features, like the location of the fast flowing central stream and some of the numerous tributaries.

To derive basal properties and to adjust basal sliding parameters pure inversion methods use the observed velocity field and minimise the misfit between observation and model result. They require no or only very little information about the bedrock properties (e.g. bed type, temperature or availability of basal water) and result in a very good representation of the flow for the time of observation. The derived basal sliding parameters then contain not

only processes related to sliding but all assumptions and approximations of the applied flow model as the surface flow is a superposition of ice deformation and basal motion. Inversion methods are therefore not sufficient to gain the knowledge about the processes at the base and their complex interplay.

5   In comparison to the inversion methods our approach relates sliding to the physical parameter of the subglacial bed roughness. Although the measured bed roughness is only valid for a certain period as the subglacial environment ~~change~~ changes over time, we do not expect the main features to change in the near future. One important process for prognostic simulations over longer time scales could be basal erosion (Smith et al. (2012) report

10 relatively high erosion rates at PIG of $0.6\,\mathrm{m\,a}^{-1} \pm 0.3\,\mathrm{m\,a}^{-1}$), but this is beyond the scope of this work.

In this study the effective pressure at the base is only influenced by the height above buoyancy and effects only the areas that ground below ~~the sea-level~~ sea level. This is a strong restriction of the model as the sliding formulation is not connected to the very diverse

15 hydrology at the base of the glacier. A sufficiently complex/realistic hydrology model would be a great benefit for this and for every other ice flow model. In that case, it might be beneficial to separate the hydrology component from the sliding relation. However, this is beyond the scope of this work.

7   Conclusions

20 The overall motion of the fast flowing parts of PIG are dominated by basal motion. The parametrisation of basal motion is therefore crucial for simulating the flow of PIG. Especially when running prognostic simulations of the glacier and aiming at analysing the stability of the system, parametrisation of basal motion is important. We introduce two different approaches of connecting a basal sliding formulation to an actually measurable subglacial

25 parameter, the basal roughness measure. Our results show, that the roughness measure is a very useful parameter to be considered for parametrisation of basal motion at PIG, as important features of the flow field could be reproduced. Nonetheless the full complexity of

27

the problem was not captured. Our approach is a step towards a more physically based parametrisation for basal sliding, which is very important for realistic simulations of glacier dynamics.

References

Aschwanden, A. and Blatter, H.: Mathematical modeling and numerical simulation of polythermal glaciers, Journal of Geophysical Research: Earth Surface, 114, F01 027, doi:10.1029/2008JF001028, 2009.

Bamber, J., Gomez-Dans, J., , and Griggs, J.: A new 1km digital elevation model of the Antarctic derived from combined satellite radar and laser data – Part 1: Data and methods, THE CRYOSPHERE, 3, 101–111, doi:10.5194/tc-3-101-2009, 2009.

Bindschadler, R.: The importance of pressurized subglacial water in separation and sliding at the glacier bed, J GLACIOL, 29, 3–19, 1983.

Bingham, R. and Siegert, M.: Quantifying subglacial bed roughness in Antarctica: implications for ice-sheet dynamics and history, QUATERNARY SCI REV, 28, 223–236, 2009.

Bingham, R. G. and Siegert, M. J.: Radar-derived bed roughness characterization of Institute and Möller ice streams, West Antarctica, and comparison with Siple Coast ice streams, Geophysical Research Letters, 34, n/a–n/a, doi:10.1029/2007GL031483, 2007.

Bingham, R. G., Siegert, M. J., Young, D. A., and Blankenship, D. D.: Organized flow from the South Pole to the Filchner-Ronne ice shelf: An assessment of balance velocities in interior East Antarctica using radio echo sounding data, Journal of Geophysical Research: Earth Surface, 112, n/a–n/a, doi:10.1029/2006JF000556, 2007.

Blatter, H. and Hutter, K.: Polythermal conditions in Arctic glaciers, J GLACIOL, 37, 261–269, 1991.

Bohlander, J. and Scambos, T.: Antarctic coastlines and grounding line derived from MODIS Mosaic of Antarctica (MOA), National Snow and Ice Data Center, Digital media, accessed 24 April 2008., Boulder, Colorado USA, 2007.

Budd, W. and Jenssen, D.: Numerical modelling of the large-scale basal water flux under the West Antarctic Ice Sheet, in: Dynamics of the West Antarctic Ice Sheet, edited by Van der Veen, C. J. and Oerlemans, J., p. 293–320, Kluwer, Dordrecht, 1987.

Codina, R.: Comparison of some finite element methods for solving the diffusion-convection-reaction
5 equation, COMPUT METHOD APPL M, 156, 185–210, doi:10.1016/S0045-7825(97)00206-5, 1998.

Comiso, J.: Variability and Trends in Antarctic surface temperatures from in situ and satellite infrared measurements, J CLIMATE, 13, 1674–1696, 2000.

COMSOL: COMSOL Multiphysics Reference Guide, COMSOL AB, Vers. 4.3a, http://www.comsol.
10 com/(lastaccess:10August2014), 2012.

Cornford, S., Martin, D., Graves, D., Ranken, D., Le Brocq, A., Gladstone, R., Payne, A., Ng, E., and Lipscomb, W.: Adaptive mesh, finite volume modeling of marine ice sheets, J COMPUT PHYS, 232, 529–549, 2012.

Cuffey, K. M. and Paterson, W. S. B.: The Physics of Glaciers, Butterworth-Heinemann, 4th edn.,
15 2010.

Dutrieux, P., De Rydt, J., Jenkins, A., Holland, P., Ha, H., Lee, S., Steig, E., Ding, Q., Abrahamsen, E., and Schröder, M.: Strong sensitivity of Pine Island ice-shelf melting to climatic variability, SCIENCE, 343, 174–178, 2014.

Favier, L., Durand, G., Cornford, S., Gudmundsson, G., Gagliardini, O., Gillet-Chaulet, F., Zwinger,
20 T., Payne, A., and Le Brocq, A.: Retreat of Pine Island Glacier controlled by marine ice-sheet instability, NATURE CLIMATE CHANGE, 4, 117–121, doi:10.1038/NCLIMATE2094, 2014.

Fowler, A.: A sliding law for glaciers of constant viscosity in the presence of subglacial cavitation, P R SOC A, 407, 147–170, 1986.

Fox Maule, C., Purucker, M., Olsen, N., and Mosegaard, K.: Heat flux anomalies in Antarctica re-
25 vealed by satellite magnetic data, SCIENCE, 309, 464–467, 2005.

Gladstone, R., Lee, V., Rougier, J., Payne, A., Hellmer, H., Brocq, A. L., Shepherd, A., Edwards, T., Gregory, J., and Cornford, S.: Calibrated prediction of Pine Island Glacier retreat during the 21st and 22nd centuries with a coupled flowline model, EARTH PLANET SC LETT, 333-334, 191–199, 2012.

30 Glen, J.: The creep of polycrystalline ice, P R SOC A, 228, 519–538, 1955.

Greve, R. and Blatter, H.: Dynamics of Ice Sheets and Glaciers, Springer, Berlin, Heidelberg, 2009.

Gudmundsson, G., Krug, J., Durand, G., Favier, L., and Gagliardini, O.: The stability of grounding lines on retrograde slopes, THE CRYOSPHERE, 6, 1497–1505, doi:10.5194/tc-6-1497-2012, 2012.

Hauke, G. and Hughes, T. J.: A comparative study of different sets of variables for solving compressible and incompressible flows, COMPUT METHOD APPL M, 153, 1–44, doi:10.1016/S0045-7825(97)00043-1, 1998.

Helm, V., Humbert, A., and Miller, H.: Elevation and elevation change of Greenland and Antarctica derived from CryoSat-2, The Cryosphere, 8, 1539–1559, doi:10.5194/tc-8-1539-2014, 2014.

Hooke, R. L.: Principles of Glacier Mechanics, Cambridge University Press, Cambridge, 2005.

Horwath, M. and Dietrich, R.: Signal and error in mass change inferences from GRACE: the case of Antarctica, GEOPHYS J INT, 177, 849–864, 2009.

Hubbard, B., Siegert, M., and McCarroll, D.: Spectral roughness of glaciated bedrock geomorphic surfaces: implications for glacier sliding, J GEOPHYS RES, 105, 21 295–21 303, 2000.

Hughes, T.: Is the West Antarctic ice sheet disintegrating?, J GEOPHYS RES, 78, 7884–7910, 1973.

Humbert, A., Kleiner, T., Mohrholz, C., Oelke, C., Greve, R., and Lange, M.: A comparative modeling study of the Brunt Ice Shelf/Stancomb-Wills Ice Tongue system, East Antarctica, J GLACIOL, 55, 53–65, 2009.

Hutter, K.: Theoretical glaciology: Material Science of Ice and the Mechanics of Glaciers and Ice Sheets, Reidel, Tokyo, 1983.

Huybrechts, P.: The Antarctic ice sheet and environmental change: a three-dimensional modelling study, REPORTS ON POLAR RESEARCH, Alfred Wegener Institute for Polar and Marine Research, Bremerhaven, 99, 1992.

Joughin, I., Tulaczyk, S., Bamber, J., Blankenship, D., Holt, J., Scambos, T., and Vaughan, D.: Basal conditions for Pine Island and Thwaites Glaciers, West Antarctica, determined using satellite and airborne data, J GLACIOL, 55, 245–257, 2009.

Joughin, I., Smith, B., and Holland, D.: Sensitivity of 21st century sea level to ocean-induced thinning of Pine Island Glacier, Antarctica, GEOPHYS RES LETT, 37, L20 502, doi:10.1029/2010GL044819, 2010.

Kamb, B.: Sliding motion of glaciers: theory and observations, Reviews of Geophysics and Space Physics, 8, 673–728, 1970.

Karlsson, N., Rippin, D., Vaughan, D., and Corr, H.: The internal layering of Pine Island Glacier, West Antarctica, from airborne radar-sounding data, ANN GLACIOL, 50, 141–146, 2009.

Katz, R. and Worster, M.: Stability of ice-sheet grounding lines, P R SOC A, 466, 1597–1620, 2010.

Kleiner, T. and Humbert, A.: Numerical simulations of major ice streams in western Dronning Maud Land, Antarctica, under wet and dry basal conditions, J GLACIOL, 60, 215–232, 2014.

Le Brocq, A., Payne, A., and Vieli, A.: An improved Antarctic dataset for high resolution numerical ice sheet models (ALBMAP v1), EARTH SYST SCI DATA, 2, 247–260, doi:10.5194/essd-2-247-2010, 2010.

Leguy, G. R., Asay-Davis, X. S., and Lipscomb, W. H.: Parameterization of basal friction near grounding lines in a one-dimensional ice sheet model, THE CRYOSPHERE, 8, 1239–1259, doi:10.5194/tc-8-1239-2014, 2014.

Li, X., Sun, B., Siegert, M., Bingham, R., Tang, X., Zhang, D., Cui, X., and Zhang, X.: Characterization of subglacial landscapes by a two-parameter roughness index, J GLACIOL, 56, 831–836, 2010.

MacAyeal, D.: The basal stress distribution of Ice Stream E, Antarctica, inferred by control methods, J GEOPHYS RES, 97, 595–603, 1992.

Morland, L.: Thermomechanical balances of ice sheet flows, GEOPHYS ASTRO FLUID, 29, 237–266, 1984.

Morlighem, M., Rignot, E., Seroussi, H., Larour, E., Ben Dhia, H., and Aubry, D.: Spatial patterns of basal drag inferred using control methods from a full-Stokes and simpler models for Pine Island Glacier, West Antarctica, GEOPHYS RES LETT, 37, L14 502, doi:10.1029/2010GL043853, 2010.

Mouginot, J., Rignot, E., and Scheuchl, B.: Sustained increase in ice discharge from the Amundsen Sea Embayment, West Antarctica, from 1973 to 2013, GEOPHYS RES LETT, 41, 1576–1584, doi:10.1002/2013GL059069, 2014.

Nye, J.: The distribution of stress and velocity in glaciers and ice-sheets, P R SOC A, 239, 113–133, 1957.

Nye, J.: The calculation of sliding of ice over a wavy surface using Newtonian viscous approximation, P R SOC A, A311, 445–467, 1969.

Park, J., Gourmelen, N., Shepherd, A., Kim, S., Vaughan, D., and Wingham, D.: Sustained retreat of the Pine Island Glacier, GEOPHYS RES LETT, 40, 1–6, 2013.

Paterson, W.: The Physics of Glaciers, Elsevier, Oxford, 1994.

Pattyn, F.: A new three-dimensional higher-order thermomechanical ice sheet model: basic sensitivity, ice stream development, and ice flow across subglacial lakes, J GEOPHYS RES, 108, 2382, doi:10.1029/2002JB002329, 2003.

Pattyn, F., Perichon, L., Aschwanden, A., Breuer, B., de Smedt, B., Gagliardini, O., Gudmundsson, G. H., Hindmarsh, R. C. A., Hubbard, A., Johnson, J. V., Kleiner, T., Konovalov, Y., Martin, C.,

Payne, A. J., Pollard, D., Price, S., Rückamp, M., Saito, F., Souček, O., Sugiyama, S., and Zwinger, T.: Benchmark experiments for higher-order and full-Stokes ice sheet models (ISMIP–HOM), The Cryosphere, 2, 95–108, doi:10.5194/tc-2-95-2008, 2008.

Pattyn, F., Perichon, L., Durand, G., Favier, L., Gagliardini, O., Hindmarsh, R. C., Zwinger, T., Al-
5 brecht, T., Cornford, S., Docquier, D., Fürst, J., Goldberg, D., Gudmundsson, H., Humbert, A., Hutten, M., Huybrechts, P., Jouvet, G., Kleiner, T., Larour, E., Martin, D., Morlighem, M., Payne, A., Pollard, D., Rückamp, M., Rybak, O., Seroussi, H., Thoma, M., and Wilkens, N.: Grounding-line migration in plan-view marine ice-sheet models: results of the ice2sea MISMIP3d intercomparison, J GLACIOL, 59, 2163, doi:10.3189/2013JoG12J129, 2013.

10 Rignot, E.: Fast recession of a West Antarctic glacier, SCIENCE, 281, 549–551, 1998.

Rignot, E.: Ice-shelf changes in Pine Island Bay, Antarctica, 1947-2000, J GLACIOL, 48, 247–256, 2002.

Rignot, E.: Changes in West Antarctic ice stream dynamics observed with ALOS PALSAR data, GEOPHYS RES LETT, 35, L12 505, doi:10.1029/2008GL033365, 2008.

15 Rignot, E., Mouginot, J., and Scheuchl, B.: Ice flow of the Antarctic ice sheet, SCIENCE, 333, 1427–1430, 2011.

Rippin, D., Vaughan, D., and Corr, H.: The basal roughness of Pine Island Glacier, West Antarctica, J GLACIOL, 57, 67–76, 2011.

Rippin, D., Bingham, R., Jordan, T., Wright, A., Ross, N., Corr, H., Ferraccioli, F., Brocq, A. L.,
20 Rose, K., and Siegert, M.: Basal roughness of the Institute and Moller Ice Streams, West Antarctica: Process determination and landscape interpretation, Geomorphology, 214, 139–147, doi:10.1016/j.geomorph.2014.01.021, 2014.

Rückamp, M.: Eisgeometrie und Fließdynamik der subpolaren Eiskappe von King George Island (Antarktis), Ph.D. thesis, Universität Münster, Münster, 2011.

25 Schmeltz, M., Rignot, E., Dupont, T., and MacAyeal, D.: Sensitivity of Pine Island Glacier, West Antarctica, to changes in ice-shelf and basal conditions: a model study, J GLACIOL, 48, 552–558, 2002.

Seroussi, H., Morlighem, M., Rignot, E., Mouginot, J., Larour, E., Schodlok, M., and Khazendar, A.: Sensitivity of the dynamics of Pine Island Glacier, West Antarctica, to climate forcing for the next
30 50 years, The Cryosphere, 8, 1699–1710, doi:10.5194/tc-8-1699-2014, 2014.

Shepherd, A., Ivins, E. R., A, G., Barletta, V. R., Bentley, M. J., Bettadpur, S., Briggs, K. H., Bromwich, D. H., Forsberg, R., Galin, N., Horwath, M., Jacobs, S., Joughin, I., King, M. A., Lenaerts, J. T. M., Li, J., Ligtenberg, S. R. M., Luckman, A., Luthcke, S. B., McMillan, M., Meister, R., Milne, G.,

32

Mouginot, J., Muir, A., Nicolas, J. P., Paden, J., Payne, A. J., Pritchard, H., Rignot, E., Rott, H., Sandberg Sørensen, L., Scambos, T. A., Scheuchl, B., Schrama, E. J. O., Smith, B., Sundal, A. V., van Angelen, J. H., van de Berg, W. J., van den Broeke, M. R., Vaughan, D. G., Velicogna, I., Wahr, J., Whitehouse, P. L., Wingham, D. J., Yi, D., Young, D., and Zwally, H. J.: A reconciled estimate of ice-sheet mass balance, SCIENCE, 338, 1183–1189, 2012.

Siegert, M. J., Taylor, J., Payne, A. J., and Hubbard, B.: Macro-scale bed roughness of the siple coast ice streams in West Antarctica, Earth Surface Processes and Landforms, 29, 1591–1596, doi:10.1002/esp.1100, 2004.

Siegert, M. J., Taylor, J., and Payne, A. J.: Spectral roughness of subglacial topography and implications for former ice-sheet dynamics in East Antarctica, Global and Planetary Change, 45, 249 – 263, doi:10.1016/j.gloplacha.2004.09.008, 2005.

Smith, A., Bentley, C., Bingham, R., and Jordan, T.: Rapid subglacial erosion beneath Pine Island Glacier, West Antarctica, GEOPHYS RES LETT, 39, L12 501, doi:10.1029/2012GL051651, 2012.

Smith, A., Jordan, T., Ferraccioli, F., and Bingham, R.: Influence of subglacial conditions on ice stream dynamics: Seismic and potential field data from Pine Island Glacier, West Antarctica, J GEOPHYS RES, 118, 1471–1482, 2013.

Stenoien, M. and Bentley, C.: Pine Island Glacier, Antarctica: A study of the catchment using interferometric synthetic aperture radar measurements and radar altimetry, J GEOPHYS RES, 105, 21 761–21 779, 2000.

Taylor, J., Siegert, M. J., Payne, A. J., and Hubbard, B.: Regional-scale bed roughness beneath ice masses: measurement and analysis, COMPUT GEOSCI, 30, 899–908, 2004.

Vaughan, D.: West Antarctic Ice Sheet collapse - the fall and rise of a paradigm, CLIMATIC CHANGE, 91, 65–79, 2008.

Vaughan, D., Corr, H., Ferraccioli, F., Frearson, N., O'Hare, A., Mach, D., Holt, J., Blankenship, D., Morse, D., and Young, D.: New boundary conditions for the West Antarctic ice sheet: subglacial topography beneath Pine Island Glacier, GEOPHYS RES LETT, 33, L09 501, doi:10.1029/2005GL025588, 2006.

Vaughan, D., Corr, H., Bindschadler, R., Dutrieux, P., Gudmundsson, G., Jenkins, A., Newman, T., Vornberger, P., and Wingham, D.: Subglacial melt channels and fracture in the floating part of Pine Island Glacier, Antarctica, J GEOPHYS RES, 117, F03 012, doi:10.1029/2012JF002360, 2012.

Weertman, J.: On the sliding of glaciers, J GLACIOL, 3, 33–38, 1957.

Weis, M., Greve, R., and Hutter, K.: Theory of shallow ice shelves, CONTINUUM MECH THERM, 11, 15–50, 1999.

33

Wilkens, N.: Pine Island Glacier - a 3D full-Stokes model study, Ph.D. thesis, Universität Hamburg, Hamburg, http://ediss.sub.uni-hamburg.de/volltexte/2014/6735/, http://ediss.sub.uni-hamburg.de/volltexte/2014/6735/(lastaccess:18August2014), 2014.

Wingham, D., Wallis, D., and Shepherd, A.: Spatial and temporal evolution of Pine Island Glacier thinning, 1995–2006, GEOPHYS RES LETT, 36, L17 501, doi:10.1029/2009GL039126, 2009.

Wright, A. P., Young, D. A., Roberts, J. L., Schroeder, D. M., Bamber, J. L., Dowdeswell, J. A., Young, N. W., Le Brocq, A. M., Warner, R. C., Payne, A. J., Blankenship, D. D., van Ommen, T. D., and Siegert, M. J.: Evidence of a hydrological connection between the ice divide and ice sheet margin in the Aurora Subglacial Basin, East Antarctica, Journal of Geophysical Research: Earth Surface, 117, n/a–n/a, doi:10.1029/2011JF002066, 2012.

Table 1. Parameter Values

| Parameter	Value	Unit	Description
ρ_i	918	$kg\,m^{-3}$	Ice density
ρ_{sw}	1028	$kg\,m^{-3}$	Seawater density
g	9.81	$m\,s^{-2}$	Acceleration of gravity
n	3		Stress exponent
R	8.314	$J\,mol^{-1}\,K^{-1}$	Gas constant
Q	60 for $T' \leq 263.15\,K$	$kJ\,mol^{-1}$	Activation energy for creep
	139 for $T' > 263.15\,K$		(Paterson, 1994)
A_0	3.985×10^{-13} for $T' \leq 263.15\,K$	$s^{-1}\,Pa^{-3}$	Pre-exponential constant
	1.916×10^3 for $T' > 263.15\,K$		(Paterson, 1994)
T_0	273.15	K	Melting point for low pressures
β_c	9.8×10^{-8}	$K\,Pa^{-1}$	Clausius-Clapeyron constant
			(Hooke, 2005)
T_{sw}	271.15	K	Freezing temperature of seawater
ν	0.1		Submelt sliding parameter
			(Budd and Jenssen, 1987)
$\kappa(T)$	$9.828\,e^{(-5.7 \times 10^{-3}\,T\,[K^{-1}])}$	$W\,m^{-1}\,K^{-1}$	Thermal conductivity
$c_p(T)$	$152.5 + 7.122\,T\,[K^{-1}]$	$J\,kg^{-1}\,K^{-1}$	Specific heat capacity
z_{sl}	0	m	Sea level
spy	31 536 000	$s\,a^{-1}$	Seconds per year
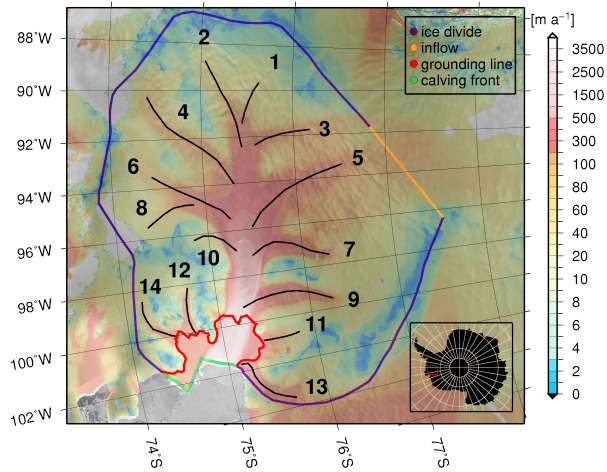
Figure 1. RADARSAT Antarctic Mapping Project (RAMP) Mosaic with the observed surface veloci-ties from Rignot et al. (2011) and the model domain of Pine Island Glacier, with the different lateral boundaries, the grounding line and the numbered tributaries indicated.
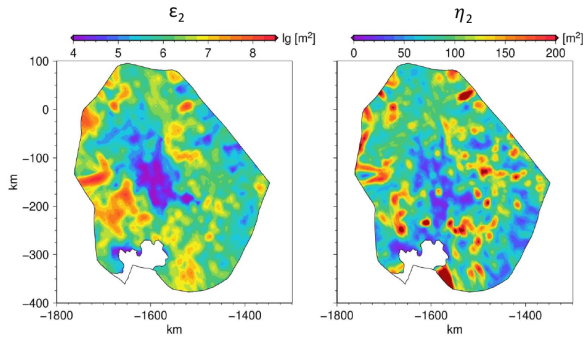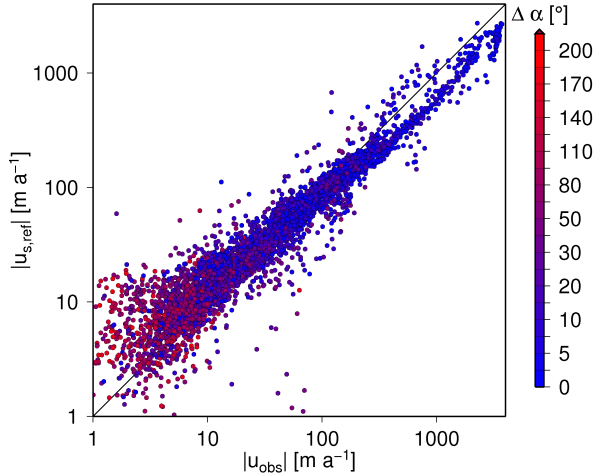
Figure 2. Calculated roughness parameters at Pine Island Glacier, given by the roughness amplitude ξ and the roughness frequency η.
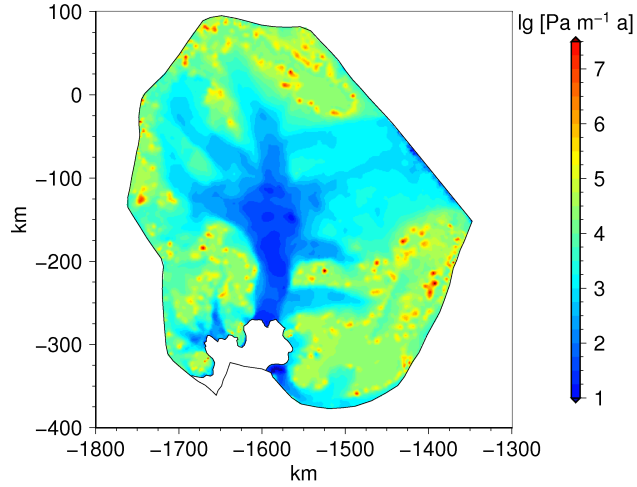
**Figure 3.** Spatial distribution of the basal sliding parameter β^2.
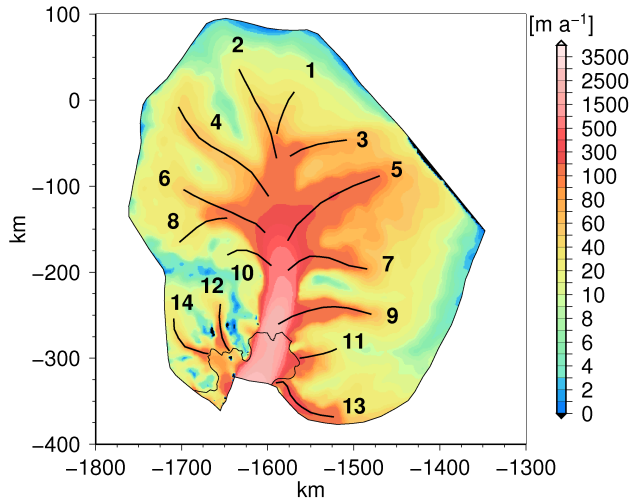
Figure 4. Surface velocity field from the reference simulation $|\boldsymbol{u}_{s,ref}|$, with the numbered tributaries.

Figure 5. Observed surface velocity field $|u_{\mathrm{obs}}|$ vs. reference surface velocity field $|u_{\mathrm{s,ref}}|$. The logarithmic scales exaggerate the spread around the low speeds. The angle offset $\Delta\alpha$ between the vectors of the surface velocity field u_{obs} and the reference surface velocity field $u_{\mathrm{s,ref}}$ is shown as the colour code.
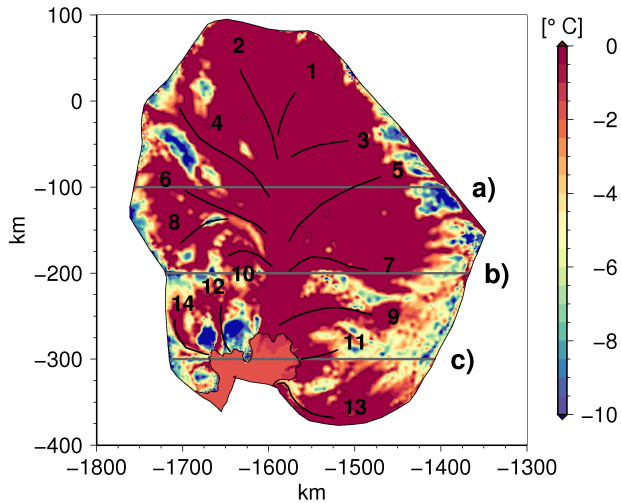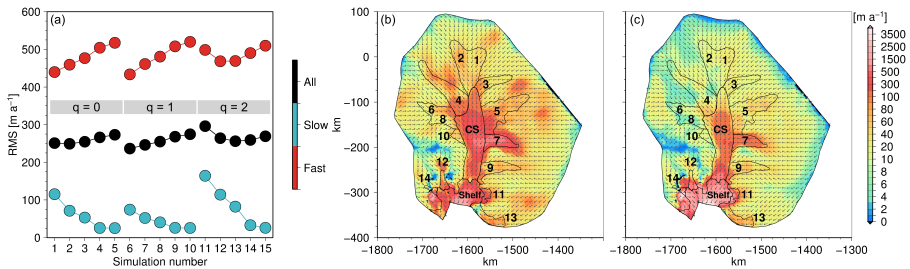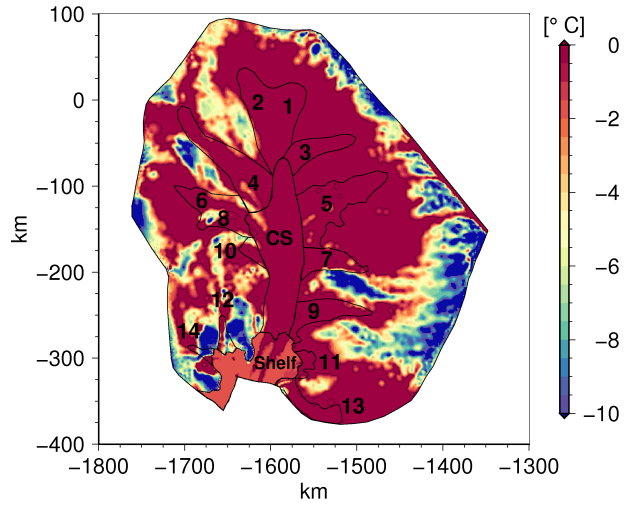
Figure 6. The basal homologous temperature from the reference simulation $T'_{b,ref}$, with tributary locations in black and the location of the vertical slices a), b) and c) in Fig. 7 in grey.
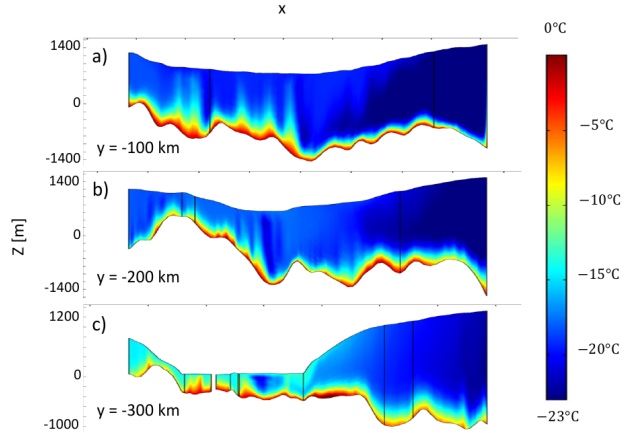
Figure 7. The internal homologous temperature from the reference simulation T'_{ref} at three vertical slices a), b) and c) (horizontal locations indicated in Fig. 6)

42

Figure 8. a) RMS error to the surface velocity field of the reference simulation versus the simulation number; b) Surface velocity field of simulation 2 with $q = 0$; c) Surface velocity field of simulation 11 with $q = 2$.

Figure 9. Basal homologous temperature of simulation 2 $T'_{b,p1q0\_2}$.
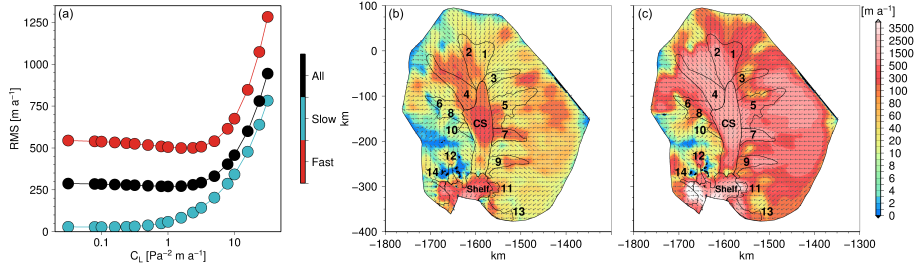
Figure 10. a) RMS error to the surface velocity field of the reference simulation versus C_L value; b) Surface velocity field with $C_L = 1 \, \text{Pa}^{-2} \, \text{m} \, \text{a}^{-1}$; c) Surface velocity field with $C_L = 31.56 \, \text{Pa}^{-2} \, \text{m} \, \text{a}^{-1}$.